Effects of surface polarity on the structure and magnetic properties of epitaxial h-YMnO3 thin films grown on MgO substrates

Journal:	*ACS Applied Electronic Materials*
Manuscript ID	el-2021-01284z.R2
Manuscript Type:	Article
Date Submitted by the Author:	n/a
Complete List of Authors:	Amrillah, Tahta; National Chiao Tung University, Department of Electrophysics Duong, My Ngoc; National Chiao Tung University, Department of Electrophysics Chen, Yu-Xun; National Chiao Tung University, Department of Electrophysics Bitla, Yugandhar; Indian Institute of Science, Physics Baqiya, Malik ; Sepuluh Nopember Institute of Technology, Physics Indah Sari, Fitri ; National Cheng Kung University Thi Quynh, Le; National Tsing Hua University, Physics Hermawan, Angga; Shinshu University - Ueda Campus, Simanjuntak , Firman Mangasa ; University of Southampton, Chen, Chia-Hao; National Synchrotron Radiation Research Center, Wu, Kaung-Hsiung; National Yang Ming Chiao Tung University, Electrophysics Juang, Jenh-Yih; National Chiao Tung University, Electrophysics

Effects of surface polarity on the structure and magnetic properties of epitaxial *h*-$YMnO_3$ thin films grown on MgO substrates

Tahta Amrillah[┼,§,*], *My Ngoc Duong*[§], *Yu-Xun Chen*[§,□], *Yugandhar Bitla*[‖], *Malik Anjelh Baqiya*[Δ], *Fitri Nur Indah Sari*[⊥], *Le Thi Quynh*[⊤], *Angga Hermawan*[┣], *Firman Mangasa Simanjuntak*[#], *Chia-Hao Chen*[□], *Kaung-Hsiung Wu*[§], *Jenh-Yih Juang*[§,*]

[┼]*Department of Nanotechnology, Faculty of Advanced Technology and Multidiscipline, Universitas Airlangga, Surabaya 60115, Indonesia*

[§]*Department of Electrophysics, National Yang Ming Chiao Tung University, Hsinchu 30010, Taiwan*

[□]*National Synchrotron Radiation Research Center (NSRRC), Hsinchu, 30076, Taiwan*

Department of Physics, School of Physical Sciences, Central University of Rajasthan, Ajmer-305817, India

[Δ]*Department of Physics, Institut Teknologi Sepuluh Nopember, Surabaya 60111, Indonesia*

[⊥]*Department of Materials Science and Engineering, National Cheng Kung University, Tainan 70101, Taiwan*

[⊤]*Department of Physics, National Tsinghua University, Hsinchu 30013, Taiwan*

[┣]*Institute of Multidisciplinary Research for Advanced Material (IMRAM), Tohoku University, 2-1-1 Katahira, Aoba-Ku, Sendai, Miyagi, Japan 980-8577*

[#]*Department of Materials Science and Engineering, National Yang Ming Chiao Tung University,*

Hsinchu 30010, Taiwan

Keywords: $YMnO_3$, thin film, surface, interface, polarity

ABSTRACT. $YMnO_3$ (YMO) thin film is one of the highly studied multiferroic materials due to its tunable crystalline structure *via* misfit strain from the substrate. This tunability involves intriguing physical phenomena that encourage further explorations for fundamental research and practical applications. The configuration of the initial atomic layers during the growth of YMO thin films plays a key role in determining their physical properties. In the present research, the correlation between the substrate's polarity and the misfit strain of the YMO films is studied comprehensively. The results showed that despite the YMO films grown on MgO (100) and MgO (111) being under the same growth conditions and having resulted in the same hexagonal crystal structure (*h*-YMO), the films do exhibit distinctly different microstructure, electronic structures, and magnetic properties. We suggest that the extent of charge accumulation induced by the surface polarity of the substrates may have resulted in a substantially different intermixing feature at the *h*-YMO/substrate interfaces, which, in turn, alters the structure and thus the physical properties of the films. Our results open up the possibility of manipulating the *h*-YMO thin film's magnetic properties by interfacial engineering without significantly altering the structure of the films which could benefit the fabrication efficiency for various next-generation electronics.

1. Introduction

Multiferroicity is a unique behavior where material could simultaneously possess magnetic and electrical orders that are intimately coupled to each other.[1–3] Various multiferroic materials, such as perovskite manganites $R\mathrm{MnO_3}$ (R: rare earth), have been found to exhibit peculiar magnetoelectric coupling mechanisms.[4–9] In particular, thin film $\mathrm{YMnO_3}$ (YMO) becomes one of the highly studied $R\mathrm{MnO_3}$ multiferroics due to its structural and physical tunability by engineering the lattice difference between the film and the substrates; the crystal structure of YMO can be tuned to have orthorhombic (o-YMO) or hexagonal (h-YMO) crystalline structure.[2,10–14] The resultant phase YMO thin film formed is mainly determined by the lattice matching with the substrates.[2,10–14] Nevertheless, several factors, such as surface energy, structure continuity, and chemical bonding at the film-substrate interface also play important role in giving rise to the final results.[15–18] The surface energy and structure continuity render a favorable crystalline direction for film growth, while the chemical bonding drives the in-plane rotation to impose the phase formation of YMO. Hence, the employment of different substrate materials can produce YMO films with various crystal structures, which, in turn, affect the physical properties of the resultant YMO films, such as defect concentration, magnetic behaviors, etc.[2,3,10–14] As multiferroic materials, YMO thin film applicable for various applications, especially next-generation electronic devices. For instance, insertion of the multiferroic layer into magnetic tunnel junction heterostructures enables the realization of a

new generation of random access memory (RAM) the so-called magnetoelectric RAM or MERAM.[19] YMO thin film is also possible to be integrated into some photovoltaic devices to induce large photocurrent density.[20] Yet, a recent study also showed that YMO could be used as a catalyst for CO_2 methanation.[21] Therefore, deeper insightful study on the formation of YMO thin film is of essential importantance to realize its promised application potential.

It is recently been found that the YMO films grown on MgO (100) and MgO (111) substrates exhibit the same (001) oriented hexagonal phase (*h*-YMO), which consists of either apical O atomic layer of MnO ion and/or Y atomic layer with formal valences of −2 and +3, respectively (Fig. 1(a)).[11] Considering the fact that the surface of MgO (100) has a non-polar surface consisting of both oxygen anions (O^{2-}) and magnesium (Mg^{2+}) cations (Fig. 1(b)),[16] while MgO (111) is terminated with polar surfaces consisting of an alternate stacking of planes of O^{2-} and Mg^{2+} (Fig. 1(c)),[17] we speculate that the growth mechanism of the *h*-YMO on both kinds of substrates might be different. For instance, in addition to lattice matching, the polarity of the substrate surface may affect the lattice registry, as well. Unfortunately, the investigation of the effects of substrate surface polarity on the formation of YMO thin films has been constantly overlooked. Consequently, the relationship between the growth mechanism and their magnetic properties remains largely unexplored. In this letter, we investigate comprehensively how the substrate surface polarity influences the detailed microstructure and the associated physical properties of *h*-YMO thin films deposited on nonpolar (100-crystal

orientation) and polar (111-crystal orientation) MgO substrates. In particular, the correlation between the interface condition and the strain effect, and its implication on the physical properties are discussed by comparing the phase and electronic structures, as well as the magnetic properties of the *h*-YMO grown on MgO (100) and MgO (111) substrates. We believe that the present study can shed some light on the importance of the choice of a proper substrate to obtain preferable YMO thin film, especially for their application in next-generation electronic devices.

2. Experimental Details

The *h*-YMO thin films investigated in this study were grown by the pulsed laser deposition (PLD) technique on MgO (100) and MgO (111) substrates. A YMO target was exposed to pulses delivered from a KrF laser (248 nm) with an energy of 260 mJ and pulse repetition rate of 5 Hz, respectively. During deposition, the substrates were maintained at 870 °C at an oxygen pressure of 180 mTorr. For comparison, a reference sample of *h*-YMO was also prepared using similar growth conditions on the non-polar YSZ (111) substrate[18,22,23] (Fig. S1 in supporting information). X-ray diffraction (XRD θ-2θ and phi-scan modes, Bruker D8 high-resolution X-ray diffractometer equipped Cu Kα1 radiation (λ = 1.5406 Å)), atomic force microscopy (AFM, Veeco Multimode 8, under ScanAsyst mode), and Raman spectroscopy (Renishaw Invia Raman Microprobe with a 633 nm He-Ne laser) were used to reveal the phase, crystal structure, and morphologies of the films. High-resolution cross-sectional transmission electron

microscopy (HR-XTEM) (JEOL JEM-F200) was performed to reveal the film/substrate interfacial structure. X-ray photoelectron spectroscopy (XPS, SPECs Phoibos 150 hemispherical energy analyzer system in Fixed Analyzer Transmission mode equipped with the Mg Kα non-monochromatic X-ray source of 1253.6 eV (300W)) was used to study the electronic structures. The C1s peak (285eV) was used to calibrate the binding energy of other chemical elements. The optical properties of the samples were measured using the photoluminescence (PL, spectrofluorophotometer (Jasco FP-8500) with the spectra being recorded using an excitation wavelength (λ) of 514.5 nm. Quantum Design® superconducting quantum-interference device (SQUID) magnetometer and magnetic property measurement system (MPMS)) were used to investigate the magnetic properties of the films.

3. Results and discussion

Fig. 2(a) displays the XRD results of the YMO thin films deposited on both MgO (100) and MgO (111) substrates, showing that both films are of hexagonal structure with (001) preferred orientation. The calculated out-of-plane lattice constant *c* is 11.435 Å and 11.392 Å for films grown on MgO (100) and MgO (111) substrates, respectively. The results imply that the *h*-YMO film on MgO (100) substrate is having about 0.313 % out-of-plane tensile strain while that on MgO (111) substrate has about 0.133 % out-of-plane compressive strain, estimated with respect to the *h*-YMO bulk values. It is noted that these values are quite consistent with those obtained by the Williamson-Hall analysis shown in Fig. S2 and Table S1, wherein a strain

factor of about 0.332% and 0.105% are obtained for YMO/MgO (100) and YMO/MgO (111), respectively. Since both *h*-YMO films are well oriented along the [001]-direction, the observed different strain states indicate that the formation of the *h*-YMO phase may have been stabilized by substantial epitaxial strain from the substrates, leading to the domain-matching epitaxy in the initial stage of growth.

The in-plane structural relation between *h*-YMO on MgO (100) and MgO (111) substrates are shown in phi-scan measurements displayed in Figs. 2(b) and (c), respectively. It is interesting to observe that the in-plane orientation of the *h*-YMO/MgO (100) exhibits a 12-fold symmetry, whereas the *h*-YMO/MgO (111) film shows a 6-fold symmetry. In Figs. 2(d) and (e), we simulate the in-plane and out-of-plane atomic arrangements of *h*-YMO on MgO (100) and MgO (111) substrates, respectively, to replicate the observed in-plane symmetry.[2] According to the principal crystallographic orientations, the *h*-YMO on MgO (100) substrate can be aligned either along MgO [011] or MgO [$0\bar{1}1$] directions; thus, the angle differences between MgO [010] and the two orientations of *h*-YMO [110] are 15° and 45°, respectively. In contrast, the *h*-YMO/MgO (111) has the in-plane lattice orientation such that MgO [211] is parallel to *h*-YMO [110] direction.[2] In this case, lattice matching holds an important key in the early stage of the *h*-YMO film growth, which tends to configure atoms on the substrate with the best lattice matching to minimize the elastic strain. On the other hand, the apical oxygens of either the MnO layer or Y layer terminated surface of *h*-YMO have to bond with the surface

atoms of the substrates. Therefore, the formation of the resultant *h*-YMO phase, in general, is a consequence of the competition between elastic strain and atomic bond formation in the first deposited layer.[2,10–15] Nevertheless, the tilted *h*-YMO crystalline structure on MgO (100) substrate may also be affected by various additional factors.[11] For instance, the polarity difference between the surface of MgO (100) and MgO (111) substrates may dictate the initial atomic bond formation of *h*-YMO differently, and hence result in different in-plane domains texturing seen in Fig. 2(b) and Fig. 2(c).

Beyond the first layers, it is important to note that epitaxial stabilization is also strongly associated with the surface energy and structural continuity resulting from *h*-YMO and the substrates. The *h*-YMO will adjust its crystalline structure to accommodate the surface energy difference between the growing film and the surface of the substrates. In particular, when the strain energy from the lattice mismatch between film and substrate accumulated from the continuously increasing film thickness, the film may follow the Stranski-Krastanov growth mechanism and switch from layer-by-layer growth to island-like growth,[24] resulting in increased surface roughness. As shown in Figs. 2(f) and 2(g) as well as in Fig. S1(b), the AFM results reveal a root-mean-square surface roughness (R_{rms}) of 0.5 nm, 1.0 nm, and 1.7 nm for films grown on MgO (111), MgO (100) and YSZ (111), respectively, suggesting that surface polarity may have resulted in distinct island nucleation kinetics in the early stage of island nucleation and contribute to the final surface morphology of the resultant films.[25]

In order to delineate the significance of the surface polarity on the early stage of island nucleation, HR-XTEM analyses were conducted. The upper and lower panels of Figs. 3(a) and 3(b) depict the HR-XTEM images of the *h*-YMO grown on MgO (100) and MgO (111) substrates, respectively. The lattice images of the *h*-YMO films grown on MgO (100) and MgO (111) substrates do exhibit quite different features at the interface. Namely, the *h*-YMO grown on the MgO (111) substrate appears to exhibit a continuous smooth interface, suggesting that the initial nucleation of the *h*-YMO is having a nearly perfect atomic registry with the substrate. In contrast, the film/substrate interface of the *h*-YMO/MgO (100) clearly shows a slightly wavy appearance with a varying feature size of about 10 nm (Fig. 3(a) left panel), indicating that an island nucleation and growth mode might have been prevailing in this case. Moreover, the corresponding fast-Fourier transform (FFT) patterns (right panels in Figs. 3(a) and 3(b)) reveal the orientation relationships between the *h*-YMO film with the MgO (100) and MgO (111) substrates are also quite different. From the FFT pattern, it turns out that, instead of typical diffraction of hexagonal crystal structure as seen in the top-most pattern shown on the right panel of Fig. 3(a) of the *h*-YMO on MgO (100) substrate, the *h*-YMO on MgO (111) substrate exhibits a cubic-like diffraction pattern, suggesting that the surface polarity of MgO (111) substrate may have forced the atomic registry to change and led to the formation of a metastable phase, such as YMn_2O_4,[15] at the interface in the initial stage of nucleation, which even persists up to more than 10 nm (Fig. 3(b), middle panel). In fact, similar surface polarity dictated film

growth had been reported previously in α-Fe_2O_3 on polar and non-polar MgO substrates[17] and *h*-YMO on the polar surface of Al_2O_3 substrate.[15] Specifically, it was found that the (2×2) reconstructed polar MgO (111) surface could facilitate a self-organized Fe_3O_4 (111) interfacial layer,[17] while both electronic and structural reconstructions were found to occur at the *h*-YMO/Al_2O_3, which even induced the formation of MnO double layer at the interface and constructed a formula-unit thick YMn_2O_4 layer with a new type of charge ordering.[15] In the present case, the differences in the interfacial structure and subsequent growth mode of the *h*-YMO films could be further complicated by the differences in the terminating orientation of the MgO substrates used.

The XPS reveals the electronic structure and chemical homogeneity within the few top-most layers from the surface of *h*-YMO films. In Fig. S3(a) of the Supplementary Information, XPS survey scans of both *h*-YMO/MgO (100) (black line) and *h*-YMO/MgO (111) (red line) films confirm the presence of Y, Mn, and O elements. The absence of any additional peaks indicates that both films are indeed free of impurity. The O 1*s* core-level spectra in Supplementary Information (Fig. S3(b)) show the presence of structural or lattice oxygen species O^{2-} of about 530.3 eV and 531.4 eV and the chemisorbed oxygen-related species at 532.5 eV and 533.7 eV for *h*-YMO/MgO (100) and *h*-YMO/MgO (111), respectively. The peaks of chemisorbed oxygen-related species may be related to the presence of oxygen vacancies in the samples.[26] Moreover, Fig. S3(c) shows the difference of the Mn 3*s* peak

energies (ΔE_{3s}) is 5.3V for each, which is consistent with the values expected for Mn (IV) and Mn (III), respectively. A linear relationship was seen between the energy separation of 3*s* splitting and the valence of Mn in oxides.[27,28] Fig. 4(a) and (b) are XPS core levels spectra of Y 3*d* and Mn 2*p* for *h*-YMO on MgO (100) and MgO (111) substrates (upper and lower panels, respectively). The doublet peak of the Y 3*d* core-level spectra centering at 156.6 eV) and 158.1 eV are corresponding to Y $3d_{5/2}$ and Y $3d_{3/2}$ levels, respectively, which are the characteristic features of the 3+ oxidation state. The Mn 2*p* core-level spectra show the Mn $2p_{3/2}$ and Mn $2p_{1/2}$ spin-orbit doublet components located at 642.1 eV and 653.6 eV, respectively, indicating the presence of Mn^{3+}.[14,15] The splitting amount of the Y 3*d* and Mn 2*p* doublets are ~1.9 eV and ~11.2 eV, respectively, which are in good agreement with data reported in the literature.[29,30] The Y 3*d* spectra can be fitted by a single component with a binding energy of Y^{3+} valence state.[31] In contrast, two components with binding energies of Mn^{3+} and Mn^{4+} valence states with an adjustable energy range of 1~1.5 eV are needed to fit the Mn 2*p* spectra[31,32], as indicated in Fig. 4 and Table 1. It is interesting to note that the Y 3*d* and Mn 2*p* doublets peaks for the *h*-YMO/MgO (111) film are located at relatively higher binding energy by a few electron volts, albeit that careful calibration was conducted prior to every measurement. Since the XPS results are sampling the film surface, thus, whether or not this is caused by the effect from interface polarity remains to be clarified.

Due to the polar characteristic of (100)-oriented *h*-YMO,[33] an interface charge

discontinuity on non-polar MgO (100) substrate is expected, which might, in turn, lead to potential divergence at the final top thin film surface[16] and cause the biding energy difference seen in Fig. 4. Alternatively, the (100)-oriented *h*-YMO has been reported to form a phase with MnO double layer on the polar surface substrate during the nucleation and create additional valence states at interfaces.[17] As shown in Table 1, the Mn oxidation state of the *h*-YMO on MgO (100) and MgO (111) are substantially different. Since the two films were grown with exactly the same deposition conditions, though the thicknesses of the samples can be slightly varied, it is reasonable to attribute the observed differences in the Mn valence states to the effect of substrate surface polarity. The larger Mn^{4+} percentage seen in *h*-YMO/MgO (111), thus, might just be a consequence of the formation of the formula-unit thick YMn_2O_4 layer, which gives rise to a new type of charge ordering and increased Mn^{4+}.[15]

Raman spectroscopy measurements were performed to understand the lattice dynamics of *h*-YMO thin-film grown on non-polar MgO (100) and polar MgO (111) substrates (black and red colors, respectively), as shown in Fig. 5(a). The *h*-YMO phase is predicted to display A_1, E_1, B_1, and E_2 symmetric Raman active modes.[34] In this work, the Raman scattering band at 680 cm^{-1} corresponds to A_1 symmetry related to stretching of apical oxygen atoms along the *c*-axis was observed in both *h*-YMO on MgO (100) and MgO (111) substrates.[34] Moreover, modes at 327 cm^{-1} and 543 cm^{-1} in *h*-YMO/MgO (111) sample are closely related to the E_2 symmetry of *h*-YMO.[35–37] These modes have also been observed in the *o*-YMO phase.[38]

Nevertheless, it is interesting to note that an additional E_2 symmetry mode exists only in *h*-YMO/MgO (111) film. This result suggests that the surface polarity of the substrate might also play a role in altering the lattice dynamics of the *h*-YMO film. The E_2 symmetry modes in *h*-YMO/MgO (111) mainly correspond to the deformation vibration or displacement of O and Mn ions.[36,37,39,40] Thus, the Raman results suggest that there is a difference in the lattice distortion of the O-Mn-O network in both *h*-YMO on MgO (100) and MgO (111) substrates. We speculate that, similar to that observed in *h*-YMO on polar Al_2O_3 (Al^{3+} layer termination) substrate mentioned above,[15] an interface reconstruction might have occurred in *h*-YMO/MgO (111) system and activated the E_2 symmetry mode seen in Fig. 5(a).

We also perform the photoluminescence (PL) spectroscopy to further explore how the surface polarity-dictated arrangement of Mn^{3+} ions affects the physical properties, in particular the electronic properties of *h*-YMO. PL is a direct and straightforward method for probing the intra-atomic Mn^{3+} states, the energies, transition probabilities, and related carrier dynamics in *h*-YMO.[41] The room-temperature PL spectra of *h*-YMO on MgO (100) and MgO (111) substrates are shown in Fig. 5(b). An additional PL peak at 3.11 eV is clearly evident in the *h*-YMO/MgO (111) sample, which has been conceived to arise from intra-atomic Mn^{3+} PL associated with magnetic spin order.[41,42] This additional PL peak could be considered as electron-hole separation from the peculiar MnO double layer formed due to electronic and structural reconstructions at the interface of *h*-YMO on polar surface MgO (111) substrate.

To understand the effect of surface polarity of MgO substrate on the magnetic properties of *h*-YMO, temperature and magnetic field-dependent magnetizations (M-T and M-H, respectively) have been examined. The M-T in zero-field-cooled (ZFC) and field-cooled (FC) modes under an external field of 500 Oe applied along in-plane of *h*-YMO thin films on MgO (100) and MgO (111) substrates are depicted in Figs. 6(a) and (b), respectively. For comparison, the M-T of *h*-YMO/YSZ (111) is shown in Fig. S4(a) in supporting information as a reference. A small hump associated with disorder-coupled spin reorientation at spin reorientation temperature T_{SR} is observed at ~28 K in *h*-YMO/MgO (100) and ~40 K in *h*-YMO/YSZ (111) (Fig. S4(a)).[2,10] Different strains imposed by the non-polar MgO (100) and YSZ (111) substrates on *h*-YMO thin films are believed to be responsible for T_{SR} difference. The strong spin-lattice coupling of *h*-YMO is affected by the in-plane strain, which distorts the lattice structure and thus, modifies the Mn–O–Mn super-exchange interaction in the in-plane.[2] However, no sign of discernible T_{SR} was observed in *h*-YMO/MgO (111) as shown in Fig. 6(b). We speculate that this might be due to the formation of the MnO double layer as being suggested by the XPS, Raman, and PL results. Moreover, the antiferromagnetic transition temperature T_N of the *h*-YMO on MgO (100) and MgO (111) substrates obtained from the Kouvel-Fischer plot shown in Fig. 6(c) is about 32 K and 42 K, respectively, while T_N = 40 K for the *h*-YMO/YSZ (111) is shown in Fig. S4(b). Considering that the in-plane strain estimated from the lattice mismatch between *h*-YMO and MgO (100), MgO (111), and YSZ (111)

substrates are about −0.29 %, +0.49%, and +1.01%, respectively.[2] It appears that the T_N of *h*-YMO does not have a consistent trend if the strain alone is considered. Therefore, there must be some other factors that modulate the magnetic properties of *h*-YMO grown on MgO (100), MgO (111), and YSZ (111) substrates. For instance, previous work showed that polar interface interactions induce a self-organized buffer layer that persists after growth, creating a defect structure and metastable magnetic state at the interface.[17] This metastable magnetic state will affect the magnetoelastic interactions as well as the local crystal field of the Mn^{3+} ions and further influences the magnetic spin ordering in *h*-YMO/MgO (111).[17,43]

The room temperature *M-H* hysteresis loops of *h*-YMO on MgO (100) and MgO (111) substrates are displayed in Fig. 6(d), showing a substantial difference in magnetic saturation, albeit the coercivity field and remanence magnetization are similar. It should be emphasized that the samples are synthesized at the same time with essentially identical growth conditions, despite that the resulting film thickness does vary slightly. Thus, the magnetic properties were calculated with respect to each individual thickness of the samples. The modulation of magnetic properties of the films grown on substrates with different surface polarities should be closely related to the differences in crystal and electronic structures at the substrate-film interfacial region.[17,44] In the polar film-substrate interfaces the emergence of metastable magnetic states associated with the peculiar in-plane domain structure may have resulted in mixed ferri/antiferromagnetic coupling and induced exchange interaction that eventually lead

to the increase in magnetic saturation.[12,17,45,46] In addition, the electrical charge-accumulation effect induced by the built-in electric field of the magnetic metastable phase at the interfaces may also result in various degrees of intermixing at the interface and modulate the electron density, giving rise to the variation of T_{SR} and T_N, as shown in Fig. 6(a),(b), and (c).[44]

Conclusions

The present study evidently revealed that the surface polarity of the substrate could significantly affect the phase stabilization of the *h*-YMO. Specifically, the surface polarity of the substrate induces the nucleation of a metastable phase during the initial growth. Such effect persists to exhibit profound influences on the growth mode, phase composition, and physical properties of the resultant *h*-YMO films. Our results imply an avenue for modulating physical properties by crafting the interfacial structures utilizing polar and non-polar substrates. These results also provide a strategy to design a delicate thin film-substrate functional interface and are expected to serve as an ideal test platform for advanced spintronics research studies for the realization of multiferroic-based electronic device applications.

FIGURES

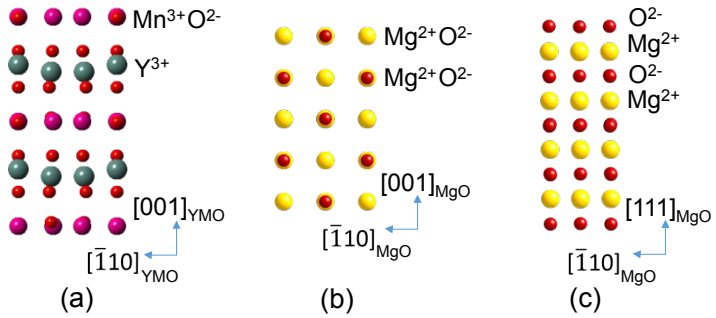

Fig. 1. The side-view atomic arrangement of (a) *h*-YMO, (b) MgO (100), and (c) MgO (111).

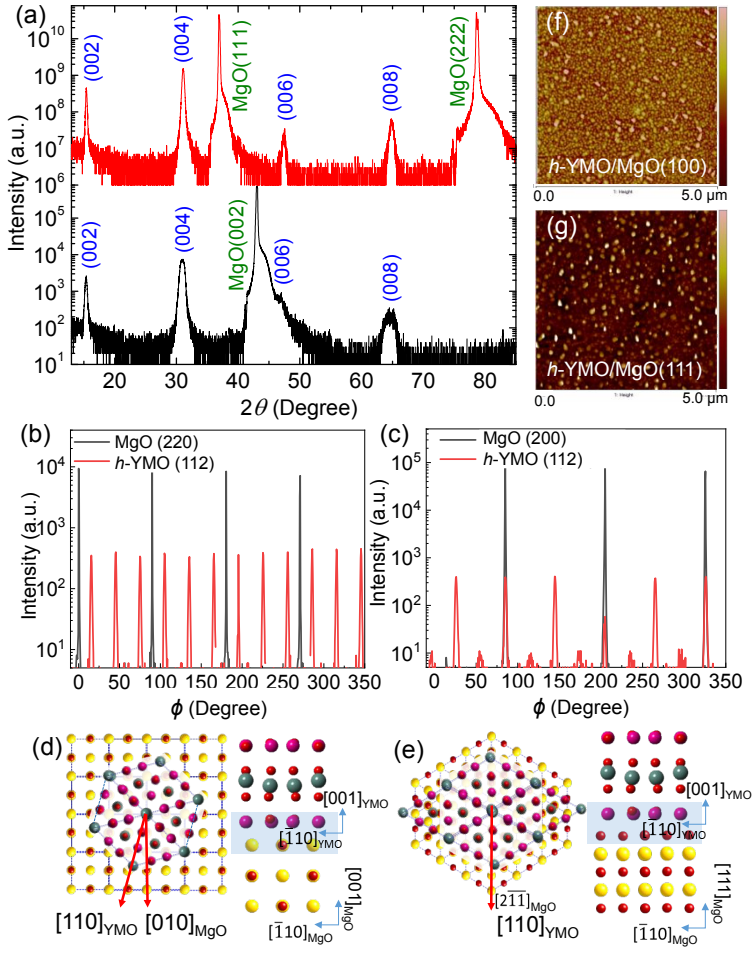

Fig. 2. (a) XRD and (b)-(c) Phi-scan results of *h*-YMO thin film grown on MgO (100) and MgO (111) substrates, respectively. Simulated in-plane and out-of-plane atomic arrangements of *h*-YMO grown on (d) MgO (100) and (e) MgO (111) substrates. AFM results show the surface morphology of *h*-YMO grown on (f) MgO (100) and (g) MgO (111) substrates.

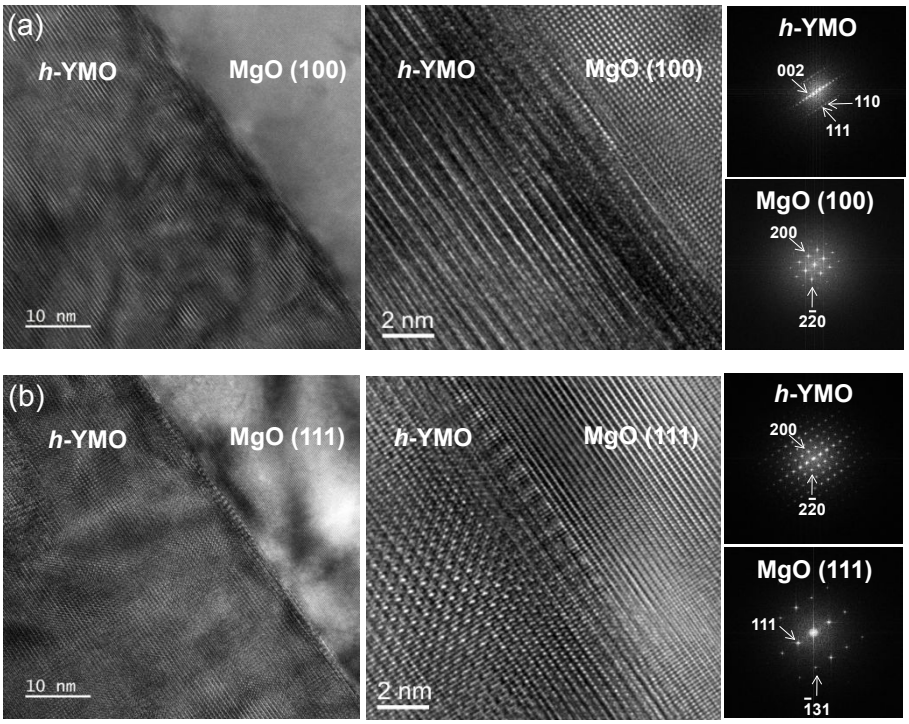

Fig. 3. (a) and (b) are crossectional TEM results as well as corresponding FFT patterns of *h*-YMO grown on MgO (100) and MgO (111) substrates, respectively.

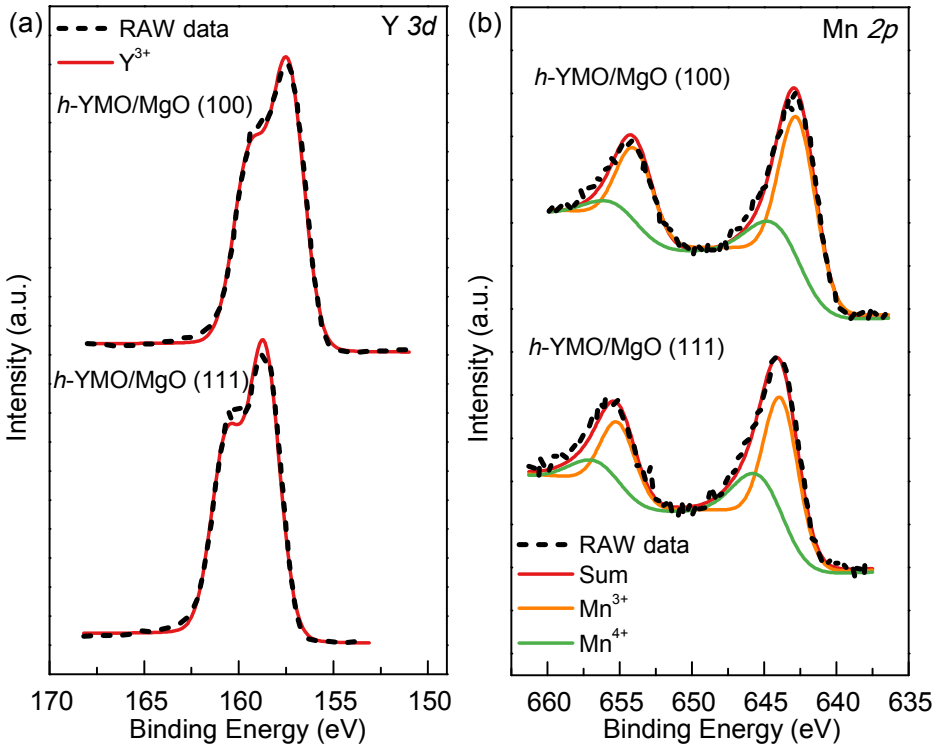

Fig. 4. XPS core levels spectra of (a) Y 3*d* and (b) Mn 2*p*, revealing the electronic structures

of YMO grown on MgO (100) and MgO (111) substrates (upper and lower panels, respectively).

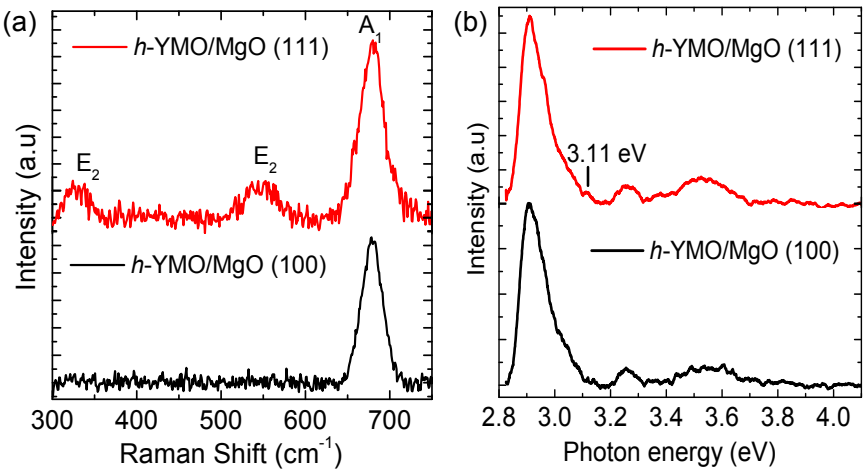

Fig. 5. (a) Raman spectroscopy and (b) photoluminescence measurements of *h*-YMO on MgO (100) (black line) and MgO (111) (red line) substrates at room temperature.

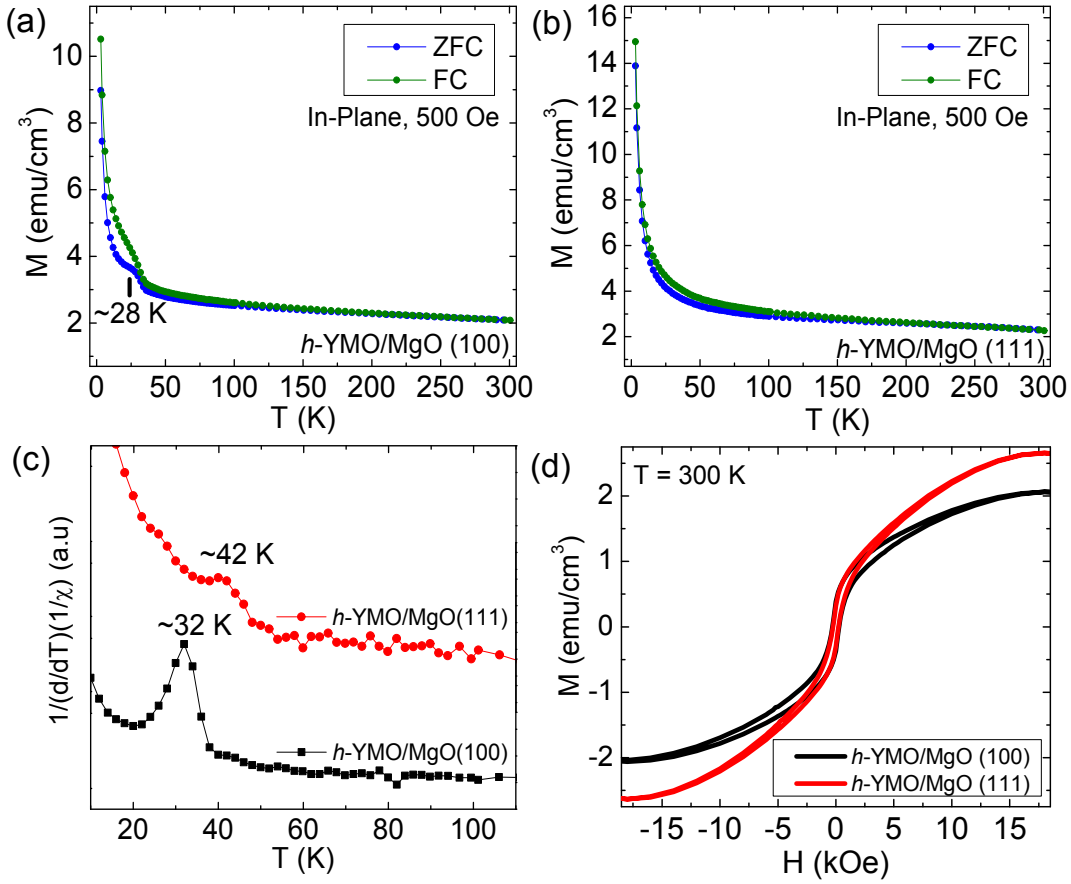

Fig. 6. Temperature-dependent magnetic measurements of *h*-YMO grown on (a) MgO (100) and (b) MgO (111) substrates. (c) Kouvel-Fischer plots from FC curve of M-T measurements.

(d) The room temperature (T = 300 K) M-H hysteresis loops of *h*-YMO grown on MgO (100) (black line) and MgO (111) (red line) substrates.

TABLE

Table 1. Fitting results of XPS measurement YMO/MgO (100) and YMO/MgO (111)

Sample	YMO/MgO (100)	YMO/MgO (111)
Element	Quant./at.%	Quant./at.%
Mn^{3+}	73.68	67.53
Mn^{4+}	23.32	32.47

AUTHOR INFORMATION

Corresponding Author

* Tahta Amrillah; tahta.amrillah@ftmm.unair.ac.id, jyjuang@g2.nctu.edu.tw

Present Addresses

Department of Nanotechnology, Faculty of Advanced Technology and Multidiscipline, Universitas Airlangga, Surabaya 60115, Indonesia

Author Contributions

The scientific work was designed by T. A and J. Y. J. All samples were prepared by T. A. XRD and AFM were done by T. A. M. N. D., Y. X. C. and C. H. C. responsible for XPS and magnetic measurements, A. H. responsible for PL measurements, M. A. B. is responsible for magnetic measurement, L. T. Q. for Phi-scan and TEM, F.N.I.S responsible for Raman measurement. The manuscript was written through the contribution of T.A, Y.B, F.M.S, K.H.W, and J.Y.J. All authors have given approval to the final version of the manuscript.

Funding Sources

Universitas Airlangga, under grand number 399/UN3.14/PT/2020

The Ministry of Science and Technology of Taiwan, under Grant Nos.: MOST 103-2112-M-009-015-MY3, 104-2628-E-009-005-MY2, 106-2112-M-009-013-MY3 and 109-2112-M-009-014-MY2

ACKNOWLEDGMENTS

The authors gratefully acknowledge the financial support of Airlangga University under Grant "Hibat Riset Mandat Muda" and the Ministry of Science and Technology of Taiwan, under Grant Nos.: MOST 103-2112-M-009-015-MY3, 104-2628-E-009-005-MY2, 106-2112-M-009-013-MY3 and 109-2112-M-009-014-MY2.

Supporting Information

XRD and AFM results of *h*-YMO grown on YSZ (111) substrate, Fitting results of Williamson-Hall analysis plot of the *h*-YMO/MgO (100), *h*-YMO/MgO (111), and *h*-YMO/YSZ (111) thin films, Plot of β_{hkl} cosθ vs sinθ of *h*-YMO/MgO (100), *h*-YMO/MgO (111), and *h*-YMO/YSZ (111) thin films, XPS survey scans, the O 1*s* and Mn 3*s* core-level spectra of *h*-YMO/MgO (100) and *h*-YMO/MgO (111) thin films, M-T measurement of *h*-YMO/YSZ (111) using similar measurements parameter of *h*-YMO grows on MgO (100) and MgO (111) substrates. Kouvel-Fischer plot from FC curve of M-T measurements of *h*-YMO/YSZ (111)

REFERENCES

(1) Kumagai, Y.; Spaldin, N. A. Structural Domain Walls in Polar Hexagonal Manganites. *Nat Commun* **2013**, *4* (1), 1540. https://doi.org/10.1038/ncomms2545.

(2) Wu, K. H.; Chen, H.-J.; Hsieh, C. C.; Luo, C. W.; Uen, T. M.; Lin, J.-Y.; Juang, J. Y. Epitaxial-Strain Effects on Electronic Structure and Magnetic Properties of Hexagonal $YMnO_3$ Thin Films Studied by Femtosecond Spectroscopy. *J Supercond Nov Magn* **2013**, *26* (4), 801–807. https://doi.org/10.1007/s10948-012-2037-8.

(3) Amrillah, T.; Bitla, Y.; Shin, K.; Yang, T.; Hsieh, Y.-H.; Chiou, Y.-Y.; Liu, H.-J.; Do, T. H.; Su, D.; Chen, Y.-C.; Jen, S.-U.; Chen, L.-Q.; Kim, K. H.; Juang, J.-Y.; Chu, Y.-H. Flexible Multiferroic Bulk Heterojunction with Giant Magnetoelectric Coupling *via* van Der Waals Epitaxy. *ACS Nano* **2017**, *11* (6), 6122–6130.

https://doi.org/10.1021/acsnano.7b02102.

(4) Catalan, G.; Scott, J. F. Physics and Applications of Bismuth Ferrite. *Adv. Mater.* **2009**, *21* (24), 2463–2485. https://doi.org/10.1002/adma.200802849.

(5) Amrillah, T.; Vandrangi, S. K.; Bitla, Y.; Do, T. H.; Liao, S.-C.; Tsai, C.-Y.; Chin, Y.-Y.; Liu, Y.-T.; Lin, M.-L.; He, Q.; Lin, H.-J.; Lee, H.-Y.; Lai, C.-H.; Arenholz, E.; Juang, J.-Y.; Chu, Y.-H. Tuning the Magnetic Properties of Self-Assembled $BiFeO_3$ – $CoFe_2O_4$ Heteroepitaxy by Magneto-Structural Coupling. *Nanoscale* **2016**, *8* (16), 8847–8854. https://doi.org/10.1039/C5NR09269H.

(6) Gich, M.; Fina, I.; Morelli, A.; Sánchez, F.; Alexe, M.; Gàzquez, J.; Fontcuberta, J.; Roig, A. Multiferroic Iron Oxide Thin Films at Room Temperature. *Adv. Mater.* **2014**, *26* (27), 4645–4652. https://doi.org/10.1002/adma.201400990.

(7) Choi, Y. J.; Yi, H. T.; Lee, S.; Huang, Q.; Kiryukhin, V.; Cheong, S.-W. Ferroelectricity in an Ising Chain Magnet. *Phys. Rev. Lett.* **2008**, *100* (4), 047601. https://doi.org/10.1103/PhysRevLett.100.047601.

(8) Alexe, M.; Ziese, M.; Hesse, D.; Esquinazi, P.; Yamauchi, K.; Fukushima, T.; Picozzi, S.; GÃ¶sele, U. Ferroelectric Switching in Multiferroic Magnetite (Fe_3O_4) Thin Films. *Adv. Mater.* **2009**, *21* (44), 4452–4455. https://doi.org/10.1002/adma.200901381.

(9) Amrillah, T.; Chen, Y.-X.; Duong, M. N.; Abdussalam, W.; Simanjuntak, F. M.; Chen, C.-H.; Chu, Y.-H.; Juang, J.-Y. Effects of Pillar Size Modulation on the Magneto-Structural Coupling in Self-Assembled $BiFeO_3$ –$CoFe_2O_4$ Heteroepitaxy. *CrystEngComm* **2020**, *22* (3), 435–440. https://doi.org/10.1039/C9CE01573F.

(10) Hsieh, C. C.; Lin, T. H.; Shih, H. C.; Hsu, C.-H.; Luo, C. W.; Lin, J.-Y.; Wu, K. H.; Uen, T. M.; Juang, J. Y. Magnetic Ordering Anisotropy in Epitaxial Orthorhombic Multiferroic $YMnO_3$ Films. *J. Appl. Phys.* **2008**, *104* (10), 103912. https://doi.org/10.1063/1.3021112.

(11) Posadas, A.; Yau, J.-B.; Ahn, C. H.; Han, J.; Gariglio, S.; Johnston, K.; Rabe, K. M.; Neaton, J. B. Epitaxial Growth of Multiferroic $YMnO_3$ on GaN. *Appl. Phys. Lett.* **2005**, *87* (17), 171915. https://doi.org/10.1063/1.2120903.

(12) Deng, S.; Cheng, S.; Liu, M.; Zhu, J. Modulating Magnetic Properties by Tailoring In-Plane Domain Structures in Hexagonal $YMnO_3$ Films. *ACS Appl. Mater. Interfaces* **2016**, *8* (38), 25379–25385. https://doi.org/10.1021/acsami.6b08024.

(13) Marti, X.; Skumryev, V.; Cattoni, A.; Bertacco, R.; Laukhin, V.; Ferrater, C.; García-Cuenca, M. V.; Varela, M.; Sánchez, F.; Fontcuberta, J. Ferromagnetism in Epitaxial Orthorhombic YMnO3 Thin Films. *J. Magn. Magn. Mater.* **2009**, *321* (11), 1719–1722. https://doi.org/10.1016/j.jmmm.2009.02.025.

(14) Yi, W.-C.; Choe, J.-S.; Moon, C.-R.; Kwun, S.-I.; Yoon, J.-G. Ferroelectric Characterization of Highly (0001)-Oriented $YMnO_3$ Thin Films Grown by Chemical Solution Deposition. *Appl. Phys. Lett.* **1998**, *73* (7), 903–905.

https://doi.org/10.1063/1.122443.

(15) Cheng, S.; Xu, C.; Deng, S.; Han, M.-G.; Bao, S.; Ma, J.; Nan, C.; Duan, W.; Bellaiche, L.; Zhu, Y.; Zhu, J. Interface Reconstruction with Emerging Charge Ordering in Hexagonal Manganite. *Sci. Adv.* **2018**, *4* (5), eaar4298. https://doi.org/10.1126/sciadv.aar4298.

(16) Albar, A.; Schwingenschlögl, U. Polar Catastrophe at the MgO(100)/SnO_2(110) Interface. *J. Mater. Chem. C* **2016**, *4* (47), 11129–11134. https://doi.org/10.1039/C6TC04264C.

(17) Cheung, S. H.; Celik-Aktas, A.; Dey, P.; Pande, K.; Weinert, M.; Kabius, B.; Keavney, D. J.; Lazarov, V. K.; Chambers, S. A.; Gajdardziska-Josifovska, M. Effects of Unreconstructed and Reconstructed Polar Surface Terminations on Growth, Structure, and Magnetic Properties of Hematite Films. *Phys. Rev. B* **2012**, *85* (4), 045405. https://doi.org/10.1103/PhysRevB.85.045405.

(18) Guo, Y.; Inoue, S.; Kobayashi, A.; Ohta, J.; Fujioka, H. Theoretical Investigation of the Polarity Determination for *c* -Plane InN Grown on Yttria-Stabilized Zirconia (111) Substrates with Yttrium Surface Segregation. *Appl. Phys. Express* **2013**, *6* (2), 021002. https://doi.org/10.7567/APEX.6.021002.

(19) Chu, Y.-H.; Martin, L. W.; Holcomb, M. B.; Gajek, M.; Han, S.-J.; He, Q.; Balke, N.; Yang, C.-H.; Lee, D.; Hu, W.; Zhan, Q.; Yang, P.-L.; Fraile-Rodríguez, A.; Scholl, A.; Wang, S. X.; Ramesh, R. Electric-Field Control of Local Ferromagnetism Using a Magnetoelectric Multiferroic. *Nature Mater* **2008**, *7* (6), 478–482. https://doi.org/10.1038/nmat2184.

(20) Tian, M.; Li, Y.; Wang, G.; Hao, X. Large Photocurrent Density in Polycrystalline Hexagonal YMnO3 Thin Film Induced by Ferroelectric Polarization and the Positive Driving Effect of Grain Boundary. *Solar Energy Materials and Solar Cells* **2021**, *224*, 111009. https://doi.org/10.1016/j.solmat.2021.111009.

(21) González-Castaño, M.; de Miguel, J. C. N.; Penkova, A.; Centeno, M. A.; Odriozola, J. A.; Arellano-Garcia, H. Ni/$YMnO_3$ Perovskite Catalyst for CO_2 Methanation. *Applied Materials Today* **2021**, *23*, 101055. https://doi.org/10.1016/j.apmt.2021.101055.

(22) Ballabio, G.; Bernasconi, M.; Pietrucci, F.; Serra, S. Ab Initio Study of Yttria-Stabilized Cubic Zirconia Surfaces. *Phys. Rev. B* **2004**, *70* (7), 075417. https://doi.org/10.1103/PhysRevB.70.075417.

(23) Vonk, V.; Khorshidi, N.; Stierle, A.; Dosch, H. Atomic Structure and Composition of the Yttria-Stabilized Zirconia (111) Surface. *Surface Science* **2013**, *612*, 69–76. https://doi.org/10.1016/j.susc.2013.02.014.

(24) Martin, L. W.; Chu, Y.-H.; Ramesh, R. Advances in the Growth and Characterization of Magnetic, Ferroelectric, and Multiferroic Oxide Thin Films. *Materials Science and Engineering: R: Reports* **2010**, *68* (4–6), 89–133.

https://doi.org/10.1016/j.mser.2010.03.001.

(25) Yu, Y.-M.; Liu, B.-G. Contrasting Morphologies of O-Rich ZnO Epitaxy on Zn- and O-Polar Thin Film Surfaces: Phase-Field Model. *Phys. Rev. B* **2008**, *77* (19), 195327. https://doi.org/10.1103/PhysRevB.77.195327.

(26) Wan, F.; Lin, X.; Bai, X.; Han, X.; Song, K.; Zheng, J.; Cao, C. Crystalline Structure and Dielectric Properties of Multiferroic Cr-Doped $YMnO_3$. *J Mater Sci: Mater Electron* **2016**, *27* (3), 3082–3087. https://doi.org/10.1007/s10854-015-4133-6.

(27) Galakhov, V. R.; Demeter, M.; Bartkowski, S.; Neumann, M.; Ovechkina, N. A.; Kurmaev, E. Z.; Lobachevskaya, N. I.; Mukovskii, Ya. M.; Mitchell, J.; Ederer, D. L. Mn 3 s Exchange Splitting in Mixed-Valence Manganites. *Phys. Rev. B* **2002**, *65* (11), 113102. https://doi.org/10.1103/PhysRevB.65.113102.

(28) Marti, X.; Skumryev, V.; Cattoni, A.; Bertacco, R.; Laukhin, V.; Ferrater, C.; García-Cuenca, M. V.; Varela, M.; Sánchez, F.; Fontcuberta, J. Ferromagnetism in Epitaxial Orthorhombic $YMnO_3$ Thin Films. *J. Magn. Magn. Mater.* **2009**, *321* (11), 1719–1722. https://doi.org/10.1016/j.jmmm.2009.02.025.

(29) Crist, B. V. Handbooks of Monochromatic XPS Spectra. *JohnWiley & Sons, New York* **1999**, *1*, 331.

(30) *Handbook of X-Ray Photoelectron Spectroscopy: A Reference Book of Standard Spectra for Identification and Interpretation of XPS Data*; Moulder, J. F., Stickle, W. F., Sobol, P. E., Bomben, K. D., Chastain, J., King Jr., R. C., Physical Electronics, Incorporation, Eds.; Physical Electronics: Eden Prairie, Minn., 1995.

(31) Kochur, A. G.; Kozakov, A. T.; Googlev, K. A.; Nikolskii, A. V. X-Ray Photoelectron Study of Temperature Effect on the Valence State of Mn in Single Crystal $YMnO_3$. *Journal of Electron Spectroscopy and Related Phenomena* **2014**, *195*, 1–7. https://doi.org/10.1016/j.elspec.2014.04.007.

(32) Wan, F.; Lin, X.; Bai, X.; Han, X.; Song, K.; Zheng, J.; Cao, C. Crystalline Structure and Dielectric Properties of Multiferroic Cr-Doped $YMnO_3$. *J Mater Sci: Mater Electron* **2016**, *27* (3), 3082–3087. https://doi.org/10.1007/s10854-015-4133-6.

(33) Cheng, S.; Deng, S. Q.; Yuan, W.; Yan, Y.; Li, J.; Li, J. Q.; Zhu, J. Disparity of Secondary Electron Emission in Ferroelectric Domains of $YMnO_3$. *Appl. Phys. Lett.* **2015**, *107* (3), 032901. https://doi.org/10.1063/1.4927205.

(34) Kumar, M.; Phase, D. M.; Choudhary, R. J. Structural, Ferroelectric and Dielectric Properties of Multiferroic $YMnO_3$ Synthesized via Microwave Assisted Radiant Hybrid Sintering. *Heliyon* **2019**, *5* (5), e01691. https://doi.org/10.1016/j.heliyon.2019.e01691.

(35) Iliev, M. N.; Lee, H.-G.; Popov, V. N.; Abrashev, M. V.; Hamed, A.; Meng, R. L.; Chu, C. W. Raman- and Infrared-Active Phonons in Hexagonal $YMnO_3$: Experiment and Lattice-Dynamical Calculations. *Phys. Rev. B* **1997**, *56* (5), 2488–2494.

https://doi.org/10.1103/PhysRevB.56.2488.

(36) Vermette, J.; Jandl, S.; Mukhin, A. A.; Ivanov, V. Y.; Balbashov, A.; Gospodinov, M. M.; Pinsard-Gaudart, L. Raman Study of the Antiferromagnetic Phase Transitions in Hexagonal Y MnO_3 and $LuMnO_3$. *J. Phys.: Condens. Matter* **2010**, *22* (35), 356002. https://doi.org/10.1088/0953-8984/22/35/356002.

(37) Fukumura, H.; Matsui, S.; Harima, H.; Kisoda, K.; Takahashi, T.; Yoshimura, T.; Fujimura, N. Raman Scattering Studies on Multiferroic $YMnO_3$. *J. Phys.: Condens. Matter* **2007**, *19* (36), 365239. https://doi.org/10.1088/0953-8984/19/36/365239.

(38) Todorov, N. D.; Abrashev, M. V.; Ivanov, V. G.; Tsutsumanova, G. G.; Marinova, V.; Wang, Y.-Q.; Iliev, M. N. Comparative Raman Study of Isostructural $YCrO_3$ and $YMnO_3$: Effects of Structural Distortions and Twinning. *Phys. Rev. B* **2011**, *83* (22), 224303. https://doi.org/10.1103/PhysRevB.83.224303.

(39) Karoblis, D.; Zarkov, A.; Garskaite, E.; Mazeika, K.; Baltrunas, D.; Niaura, G.; Beganskiene, A.; Kareiva, A. Study of Gadolinium Substitution Effects in Hexagonal Yttrium Manganite $YMnO_3$. *Sci Rep* **2021**, *11* (1), 2875. https://doi.org/10.1038/s41598-021-82621-6.

(40) Zhou, G.; Gu, X.; Xie, W.; Gao, T.; Peng, J.; Wu, X. S. Polarized Raman Scattering Studies of Hexagonal $YMnO_3$ Single Crystal. *IEEE Trans. Magn.* **2015**, *51* (11), 1–4. https://doi.org/10.1109/TMAG.2015.2438154.

(41) Nakayama, M.; Furukawa, Y.; Maeda, K.; Yoshimura, T.; Uga, H.; Fujimura, N. Correlation between the Intra-Atomic Mn^{3+} Photoluminescence and Antiferromagnetic Transition in an $YMnO_3$ Epitaxial Film. *Appl. Phys. Express* **2014**, *7* (2), 023002. https://doi.org/10.7567/APEX.7.023002.

(42) Takahashi, J.; Kohn, K.; Hanamura, E. Luminescence Spectrum from Hexagonal $YMnO_3$. *Journal of Luminescence* **2002**, *100* (1–4), 141–145. https://doi.org/10.1016/S0022-2313(02)00424-6.

(43) Bergum, K.; Okamoto, H.; Fjellvåg, H.; Grande, T.; Einarsrud, M.-A.; Selbach, S. M. Synthesis, Structure and Magnetic Properties of Nanocrystalline $YMnO_3$. *Dalton Trans.* **2011**, *40* (29), 7583. https://doi.org/10.1039/c1dt10536a.

(44) Chiba, D.; Shibata, N.; Tsukazaki, A. Co Thin Films Deposited Directly on ZnO Polar Surfaces. *Sci Rep* **2016**, *6* (1), 38005. https://doi.org/10.1038/srep38005.

(45) Amrillah, T.; Hermawan, A.; Wulandari, C. P.; Muthi'Ah, A. D.; Simanjuntak, F. M. Crafting the Multiferroic $BiFeO_3$-$CoFe_2O_4$ Nanocomposite for next-Generation Devices: A Review. *Materials and Manufacturing Processes* **2021**, 1–18. https://doi.org/10.1080/10426914.2021.1945096.

(46) Amrillah, T.; Hermawan, A.; Bitla, Y.; Baqiya, M. A.; Quynh, L. T.; Taufik, A.; Yin, S.; Juang, J.-Y. Preferentially Oriented Nanometer-Sized $CoFe_2O_4$ Mesocrystals Embedded in the $BiFeO_3$ Matrix for Opto-Magnetic Device Applications. *ACS Appl.*

Nano Mater. **2021**, acsanm.1c02804. https://doi.org/10.1021/acsanm.1c02804.

For Table of Contents Use Only

Effects of surface polarity on the structure and magnetic properties of epitaxial *h*-$YMnO_3$ thin films grown on MgO substrates

Tahta Amrillah, My Ngoc Duong, Yu-Xun Chen, Yugandhar Bitla, Malik Anjelh Baqiya, Fitri Nur Indah Sari, Le Thi Quynh, Angga Hermawan, Firman Mangasa Simanjuntak, Chia-Hao Chen, Kaung-Hsiung Wu, Jenh-Yih Juang

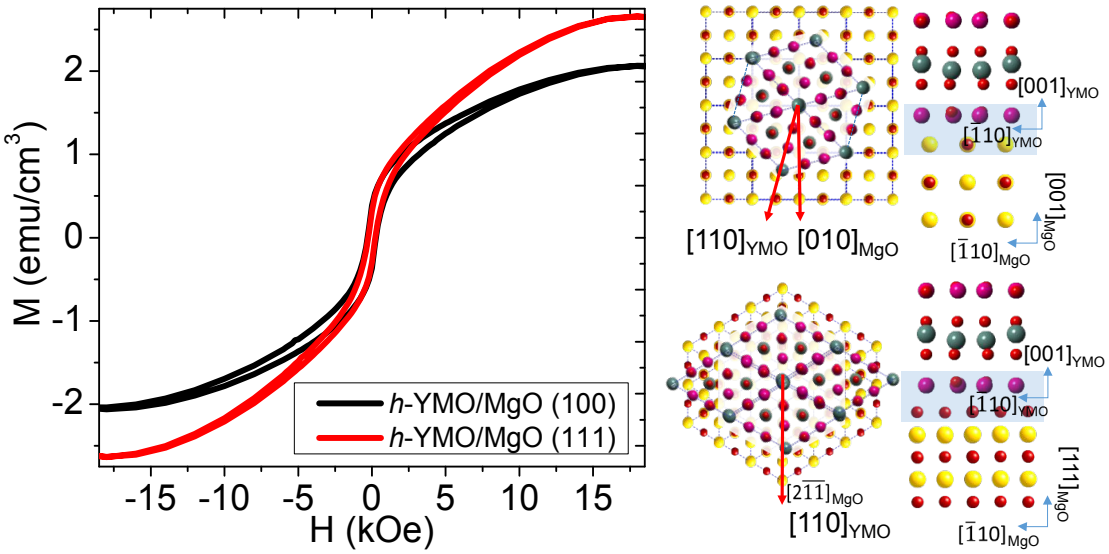

SYNOPSIS. Polar interfaces effects are of pivotal importance to determine the structure and physical properties of *h*-YMO apart from the strain-induced from the substrates.